Journal Pre-proof


# Blocking the cytohesin-2/ARF1 axis by SecinH3 ameliorates osteoclast-induced bone loss via attenuating JNK-mediated IRE1 endoribonuclease activity

Yimin Dong, Kehan Song, Pengju Wang, Jiachao Guo, Honglei Kang, Xi Tan, Binxiang Zhu, Renpeng Peng, Meipeng Zhu, Kaixu Yu, Qian Guo, Hanfeng Guan, Feng Li

PII: S1043-6618(22)00459-5

DOI: https://doi.org/10.1016/j.phrs.2022.106513

Reference: YPHRS106513

To appear in: *Pharmacological Research*

Received date: 16 August 2022
Revised date: 12 October 2022
Accepted date: 12 October 2022

Please cite this article as: Yimin Dong, Kehan Song, Pengju Wang, Jiachao Guo, Honglei Kang, Xi Tan, Binxiang Zhu, Renpeng Peng, Meipeng Zhu, Kaixu Yu, Qian Guo, Hanfeng Guan and Feng Li, Blocking the cytohesin-2/ARF1 axis by SecinH3 ameliorates osteoclast-induced bone loss via attenuating JNK-mediated IRE1 endoribonuclease activity, *Pharmacological Research,* (2022) doi:https://doi.org/10.1016/j.phrs.2022.106513

# Blocking the cytohesin-2/ARF1 axis by SecinH3 ameliorates osteoclast-induced bone loss via attenuating JNK-mediated IRE1 endoribonuclease activity

Yimin Dong MD[1#], Kehan Song MD[1#], Pengju Wang MD[1], Jiachao Guo[2], Honglei Kang MD[1], Xi Tan, MM[3], Binxiang Zhu MD[1], Renpeng Peng MD[1], Meipeng Zhu MD[1], Kaixu Yu MM[1], Qian Guo MD[1], Hanfeng Guan MD[1*], Feng Li MD[1*]

1. Department of Orthopedics, Tongji Hospital, Tongji Medical College, Huazhong University of Science and Technology, Wuhan, China.

2. Department of Pediatric Surgery, Tongji Hospital, Huazhong University of Science and Technology, Wuhan, China.

3. Department of Anesthesiology, Dongguan People's Hospital, Dongguan 5230181, Guangdong, China

# Contributed equally

*** Corresponding authors:** Hanfeng Guan, Address: Jiefang Road, Qiaokou Distract, Wuhan City, Hubei Province, China. E-mail: hguan@hust.edu.cn;

Feng Li, Address: Jiefang Road, Qiaokou Distract, Wuhan City, Hubei Province, China. E-mail, lifengmd@hust.edu.cn.

## Abstract

cytohesin-2 is a guanine nucleotide exchange factor to activate ARF1 and ARF6, which are involved in various biological processes, including signal transduction, cell differentiation, cell structure organization, and survival. Nevertheless, there is a lack of evidence revealing the role of cytohesin-2 in osteoclast differentiation and in the development of osteoporosis. In this study, we find cytohesin-2 and ARF1 positively regulate osteoclast differentiation and function. Blocking the cytohesin-2 /ARF1 axis with SecinH3 or by genetic silencing of cytohesin-2 inhibits osteoclast formation and function in vitro. In vivo treatment with SecinH3 ameliorates ovariectomy-induced osteoporosis. Mechanistically, RNA-sequencing combined with molecular biological methodologies reveal that the regulatory function of cythohesin-2/ARF1 axis in

osteoclast differentiation is mainly dependent on activating the JNK pathway. Further, in addition to the common viewpoint that JNK is activated by IRE1 via its kinase activity, we found that JNK can act upstream and regulate the endoribonuclease activity of IRE1 to promote XBP1 splicing. Both SecinH3 and silencing of cytohesin-2 inhibit JNK activation and IRE1 endoribonuclease activity, leading to the suppression of osteoclast differentiation. Taken together, our findings add new insights into the regulation between JNK and IRE1, and reveal that inhibiting the cytohesin-2/ARF1/JNK/IRE1 axis might represent a potential new strategy for the treatment of post-menopause osteoporosis.

**Keywords**

cytohesin-2; osteoclast; ARF1; JNK; IRE1; endoribonuclease activity; SecinH3;

Chemical compounds studied in this article SecinH3 (PubChem CID: 1029232); 4μ8C (PubChem CID: 12934390); SP600125 (PubChem CID: 8515); Thapsigargin (PubChem CID: 446378); NAV-2729 (PubChem CID: 2257249)

## Introduction

Post-menopause osteoporosis is an endocrine disorder characterized by decreased bone mass and increased risk of fragile fractures, especially vertebral and hip fractures [1]. With population aging, osteoporosis is associated with increased number of disabilities and deaths, representing a huge threat to the well-being of people and substantially increasing social economic burden [2]. In post-menopause osteoporosis, osteoclasts (OCs) are over-activated, with enhanced bone resorption activity, which disrupts the dynamic balance of bone resorption and formation. Inhibiting the formation and resorptive function of OCs is one of the main strategies for the treatment of osteoporosis [3]. However, due to the adverse effects and poor adherence to existing drugs, the treatment of osteoporosis is far from satisfactory [2]. Thus, exploring new therapeutic targets for osteoporosis will help to benefit patients and reduce the related burden.

OCs differentiate from bone marrow derived macrophages (BMMs) following the stimulation of macrophage colony-stimulating factor (M-CSF) and receptor activator of nuclear factor-κB (RANK) ligand (RANKL). M-CSF is a hematopoietic growth factor responsible for the proliferation of BMMs, while RANKL initiates the differentiation signaling in BMMs to form OCs [4]. Upon RANKL binding, the receptor RANK in the plasma membrane recruits the adaptor protein tumor necrosis factor receptor-associated factor 6 (TRAF6) to transduce intracellular signaling, which further activates the mitogen activated protein kinases (MAPKs), nuclear factor-κB (NF-κB), and Akt signaling pathways to promote OC differentiation and survival [5]. The MAPK pathway has three main downstream branches in the RANK signaling: the extracellular signal-related kinases (ERK) pathway, p38 pathway, and Jun amino-terminal kinases (JNK) pathway. Nuclear factor of activated T-cells cytoplasmic 1 (NFATc1), the master transcription factor of osteoclastogenesis, is then robustly amplified following these signals and translocates to the nuclei to initiate the expression of *cathepsin K* (*CTSK*), *tartrate-resistant acid phosphatase* (*TRAP*), and many other genes that are typical of OCs and are crucial for the resorptive function [5-7].

Endoplasmic reticulum (ER) stress plays an important role in OC differentiation and function [8, 9]. It occurs when unfolded proteins accumulate in the ER lumen and is harmful to cells if it lasts too long. Cells have a defensive machinery to prevent long-term ER stress, called the unfolded protein response (UPR). UPR has three branches mediated by inositol-requiring protein-1 (IRE1), activating transcription factor 6 (ATF6), and pancreatic ER kinase (PERK), respectively. Previously, we have found that PERK signaling is involved in OC differentiation and function, and inhibition of PERK can improve bone loss in OVX mice [9]. IRE1-mediated UPR is highly conserved among species. IRE1 possesses both kinase and endoribonuclease activities. The kinase activity is associated with the activation of JNK [10], while the endoribonuclease activity is augmented by the autophosphorylation of IRE1 (p-IRE1), which further converts the un-spliced mRNA of X-box binding protein 1 (*XBP1u*) into

the spliced form *XBP1s*, a process typical of p-IRE1 mediated branch of UPR [11, 12]. The IRE1/XBP1 pathway has been reported to facilitate the transcription of *NFATc1*, thus promoting OC differentiation [8]. After RANKL stimulation, the IRE1/XBP1s activity increases gradually and peaks in two days [8]. However, the JNK pathway in the RANK signaling of OC is transiently activated as early as 15 minutes after RANKL treatment [13, 14]. These temporal differences in the activation of IRE1 and JNK pathways lead us to question whether JNK can regulate the activity of IRE1.

Cytohesin proteins belong to a sub-family of the guanine nucleotide exchange factors (GEFs) that activate the adenosine diphosphate-ribosylation factor 1 and 6 (ARF1 and ARF6), two small guanine nucleotide-binding proteins of the Ras super family [15]. ARF1 and ARF6 are inactivated by binding to GDP and activated by binding to GTP. Cytohesin proteins possess a Sec7 domain, which can dissociate GDP and load GTP to ARF1 or ARF6 to activate them [15]. There are four members in the cytohesin family (cytoheisn-1, cytohesin-2, cytohesin-3, and cytohesin-4), which are involved in a wide range of biological processes, such as signal transduction, cell differentiation, cell structure organization, and survival [15]. For example, cytohesin-3 has been identified as an essential component of the PI3K-Akt pathway in transducing the insulin signaling [16], while cytohesin-2 and ARF6 act with the vacuolar proton-translocating ATPase (V-ATPase) in the endosome to facilitate endosome acidification, which is crucial for the endocytosis of extracellular particles and plasma membrane receptors [17]. In macrophage-like THP1 cells and fibroblasts, cytohesin-2 along with ARF1 controls the assembly of podosomes, structures that are crucial for integrin-mediated cell to matrix adhesion. In endothelial cells, cytohesin-2 activates ARF6 and directly binds to the adaptor protein MYD88 in the IL-1β signaling to transduce inflammatory signals [18]. Interestingly, the PI3K-Akt pathway, V-ATPase mediated acidification, and podosome formation are all important processes for the differentiation and function of OCs. However, the role of cytohesins in OCs has never been reported. Although ARF1 has been reported to regulate the migration, proliferation, and fusion of OCs [19], it remains unknow how ARF1 affects these

processes and which cytohesin is responsible for the control of ARF1 activity in OCs.

Considering the role of cytohesins and ARFs in signal transduction and in various cellular processes, we speculated that they might have a role in OC differentiation and function. The Sec7 domain can be selectively inhibited by SecinH3, an organic compound specifically blocking cytohesin-mediated ARF1 or ARF6 activation [20]. In this study, we found the cytohesin-2/ARF1 axis is involved in OC differentiation. Blocking the axis by silencing cytohesin-2 or by SecinH3 suppresses OC differentiation and resorptive function. In vivo treatment with SecinH3 attenuates bone loss in mice after ovariectomy (OVX). Mechanistically, we found that cytohesin-2 and ARF1 can activate JNK in the RANK signaling, which further regulates the endoribonuclease activity of IRE1 to promote UPR. These findings provide novel strategies for the treatment of osteoporosis by inhibiting OC differentiation via disrupting the cytohesin-2/ARF1/JNK/p-IRE1 pathway.

## Materials and methods

### 1. Reagents and antibodies

SecinH3, 4μ8C, and SP600125 were purchased from Selleck (Houston, USA). Recombinant RANKL (#462--TR) and M-CSF (#416--ML) were purchased from R&D Systems (Minnesota, USA). Antibodies against XBP1s (#12782), JNK (#9252) and p-JNK (#4668) were obtained from Cell Signaling Technology (Shanghai, China). Antibodies targeting CTSK (#ab37259) and TRAP (#ab52750) were purchased from Abcam (Cambridge, UK). Antibodies against TRAF6 (A16991), IRE1(A17940), and p-IRE1(AP1146) were provided by ABclonal (Wuhan, China). Antibodies against cytohesin-2 (67185-1-Ig) was obtained from Proteintech Group (Wuhan, China).

### 2. BMM isolation and in vitro OC differentiation assay

BMMs were obtained from the medullary space of bilateral tibias/femurs of 8-week-old C57BL/6J mice. α-MEM medium with 30 ng/ml M-CSF and 10% fetal

bovine serum (FBS) was used to culture the isolated BMMs. Sixteen hours later, the suspended cells were transferred to a new 10-cm dish and were further cultured for three days with 2 mL α-MEM supplemented per day. Cells adhering to the new dish on day 3 were BMMs and were digested with 0.25% trypsin for further use. To induce OC differentiation, BMMs were seeded onto 96-well plates at a density of $2\times10^4$ per well. Then, the cells were cultured in the presence of 75 ng/ml RANKL for five days to induce OCs.

**3. ALP staining and Mineralization assay of osteoblasts**

For the ALP staining and mineralization assay of osteoblasts, MC3T3-E1 cells were cultured in osteogenic differentiation medium containing 10 mM b-glycerophosphate, 50 μg /mL ascorbic acid, and 10 nM dexamethasone. ALP staining was performed using an alkaline phosphatase staining kit (#C3206, Beyotime, Beijing, China) on MC3T3-E1 cells after being cultured for seven days. The mineralization degree was evaluated by 1% alizarin red S staining after 21-day osteogenic differentiation. For the two staining assays, cultured cells were fixed with 4% paraformaldehyde for 15 min at room temperature, followed by washing with PBS for three times and then staining with the staining solution for 30 min. The expression of osteoblast related genes, such as *Alp*, *Runx2*, and *Ocn*, was determined by polymerase chain reaction (PCR) after osteogenic induction for seven days.

**4. Cell toxicity assay**

BMMs were seeded onto 96-well plates at a density of $5\times10^3$ per well and were cultured with 30 ng/ml M-CSF for one day. Then, the medium was replaced with fresh medium containing various concentrations of SecinH3 once daily for 1, 3, and 5 days. CCK8 assay kit (#AR1160, Boster Biotechnology, Wuhan, China) was used to examine the influence of SecinH3 on the proliferation of BMMs.

**5. TRAP staining, podosome structure staining, and pit formation assay**

For TRAP staining, BMMs were first incubated with 75 ng/ml RANKL in 96-well

plate for 5 days to induce OCs. Then, cells were washed with PBS and fixed with 4% paraformaldehyde for 15 min. The TRAP staining buffer was prepared according to the manufacturer's instructions. The buffer was added to the cells, followed by incubation at 37℃ for 1 hour. OCs were counted as TRAP-positive cells with at least three nuclei.

For podosome structure staining, OCs were induced on hydroxyapatite-coated Osteo Assay strip well plates (Corning, USA) with different concentrations of SecinH3. Then, cells were fixed with 4% paraformaldehyde, permeabilized with 0.25% Triton X-100 for 15 min, and incubated with FITC-phalloidin (#P5282, Sigma--Aldrich, St. louis, USA) at room temperature for one hour. The podosome structures, including podosome clusters and podosome belts, were counted under a fluorescence microscope and representative images were captured for each well. Finally, the cells were lysed and washed to exposure the bottom, and images of the resorption pits were obtained under a microscope. The area of resorption region was calculated using the image J software.

**6. Real-time quantitative PCR (RT-qPCR)**

The RNA of treated cells was extracted using TRIzol reagent (Takara, Japan), according to the manufacturer's instructions. For each sample, one microgram RNA was reversely transcribed into cDNA using the HiScript III All-in-one RT SuperMix Perfect for qPCR (Vazyme Biotech Co.,Ltd, Nanjing, China). Then, the cDNA was detected in RT-qPCR by using the HiScript II Q RT SuperMix for qPCR (Vazyme Biotech Co.,Ltd, Nanjing, China). All the mRNA levels of the target genes were normalized to the level of housekeeping gene β-Actin.

**7. Western blot assay**

Cells were washed and lysed with RIPA buffer containing phosphotransferase inhibitor (1%) and proteinase inhibitor (1%). The concentration of proteins was measured using the bicinchoninic acid (BCA) kit (Boster Biotechnology, Wuhan, China). Proteins were separated in 10% SDS-PAGE by electrophoresis for 1.5 h. Then,

the proteins were transferred to PVDF membranes (#IPVH00010, Millipore, Boston, USA) and were blocked with 5% BSA dissolved in TBS (with 0.1% Tween 20) at room temperature for 1 hour. Subsequently, the membranes were incubated with the primary antibodies at 4 ℃ overnight. On the next day, the membranes were incubated at room temperature with horseradish peroxidase--conjugated secondary antibodies for 1 hour, and ECL solution (#34095, Thermo Fisher Scientific, MA, USA) was used to detect the signals.

**8. RNA sequencing and data analysis**

BMMs were divided into SecinH3 (12 μM) treated group and control group, with three replicates in each group. The RNA was extracted with TRIzol reagent (Takara, Japan) and was sent to Novogene (Beijing, China) for RNA sequencing. For data analysis, we set the threshold of $|\log_2(\text{Foldchange})|$ to 0.5 to identify differentially expressed genes (DEGs) between the two groups. Based on the DEGs, we performed Kyoto Encyclopedia of Genes and Genomes (KEGG) to determine signaling pathways that were significantly changed by SecinH3 treatment. Gene Set Enrichment Analysis (GSEA) analysis was further performed to confirm the results of KEGG analysis.

**9. Adenovirus and lentivirus transfection**

Adeno-virus was used to deliver short hairpin RNA (shRNA) into BMMs to knock down the expression of cytohesin-1, -2 or -3. The knockdown and control virus were produced by ViGene Biosciences Inc (Shandong, China). Four sequences of shRNA targeting each cytohesin were constructed into one vector to enhance the knockdown efficiency, and the sequences were provided in supplementary file 1. Scramble sequences of equal length were constructed in the same vector as controls. Lentivirus transfection was used to overexpress the constitutively active mutant ARF1 (Q71L) and dominant negative mutant ARF1 (T31N). ARF1 (Q71L) contains a point mutation rendering ARF1 resistant to inactivation [21], while ARF1 (T31N) contains a mutant to restrict GDP and was resistant to activation. The plasmids were constructed by

Tsingke Biotechnology Co., Ltd (Beijing, China). For cell transfection, BMMs were incubated with adenovirus at a MOI (multiplicity of infection) of 200 per cell in complete α-MEM medium for 12 h, or with lentivirus in complete α-MEM medium containing 5 μg/ml polybrene for 24 h. The knockdown or overexpressing efficiency was determined by western blot assay.

**10. Detection of ARF1 activation**

ARF1 activation was detected using a commercial kit (#BK032-S, Cytoskeleton, Inc, Denver, USA). The kit utilizes beads conjugated with the ARF1 protein binding domain (PBD) of the effector protein GGA3 (Golgi-localized γ-ear containing, arf-binding protein 3) to capture ARF1. GGA3-PBD has been shown to specifically binding the GTP-bound form of ARF1 [22]. Before the detecting assay, we quantified total ARF1 in the cell lysates by normalizing to β-actin in the lysates per sample. Then, we incubated 300 μg total proteins in the lysates with 20 μg GGA3-PBD beads and further used western blot to detect ARF1- GTP captured by the beads. All steps adhered strictly to the instructions of the kit.

**11. Mouse model of ovariectomy (OVX) induced osteoporosis and in vivo treatment.**

The animal study protocols and procedures in this study were approved by the Ethics Committee of Tongji Hospital, Huazhong University of Science and Technology. No human participants or human samples were used in this study. Eight-week-old mice were purchased via the experimental animal center of our institute. The mice were further housed in a specific pathogen free environment with free access to sterile food and water. OVX was performed on mice at the age of eleven weeks, and drug treatment was initiated after one week of recovery from OVX surgery. For the in vivo treatment, SecinH3 was dissolved in vehicles (VEH, 10% v/v dimethyl sulfoxide + 40% v/v Polyethylene glycol 300 + 5% v/v Tween 80 + 45% v/v dd$H_2O$) and was administrated via intraperitoneal injection. Zoledronic acid disodium tetrahydrate (ZA) was used as positive control for the treatment of osteoporosis, which is a

third-generation bisphosphonate with potent anti-resorptive activity at a concentration from 0.05 to 1 mg / kg [23].

The mice were randomly divided into five groups (n = 6 for each group): sham + VEH (sham surgery and treated with vehicles); OVX+ VEH (OVX and treated with vehicles); OVX + low-dose SecinH3 (5 mg/kg); OVX + high-dose SecinH3 (10 mg/kg)， and OVX + ZA (0.05 mg/kg). The OVX model was constructed as previously reported. Briefly, the female mice were narcotized with 1% pentobarbital dissolved in normal saline. Then, the bilateral ovaries were exposed and removed via a dorsal approach. Subsequently, the incisions were sutured and disinfected. For mice in the sham group, similar procedures were performed and the incisions were sutured after exposing the ovaries. After one week of recovery from surgery, mice were peritoneally injected with SecinH3 or vehicles five days a week for six weeks. Then, the experimental mice were sacrificed, and the bilateral femurs were collected for further experiments. Before sacrifice, peripheral blood was collected from the periorbital vein. After centrifugation at 2000 rpm for 30 min, the serum was collected to detect the concentration of C-terminal telopeptide of type I collagen (CTX-1), using a commercially available Elisa kit (Bangyi Biotechnology Co., Ltd, Shanghai, China)

**12. Micro-computed tomography (μCT) and histo-morphometric analysis**

The right femur of each mouse was fixed in 4% paraformaldehyde and was subjected to μCT system (Scanco Medical) for bone morphometric analysis. The parameters were 100 kV, 98 μA, and 10 μm voxel size for femur scanning. The built-in software in the μ-CT system was used to evaluate trabeculae bone morphometric parameters, including bone volume/tissue volume (BV/TV), trabecular thickness (Tb.Th), trabecular numbers (Tb.N), trabecular space (Tb.Sp), and mean density of bone volume (mg HA /ccm). The images showing the femur trabeculae bone were then obtained after three-dimensional reconstruction. The left femurs were fixed with 4% paraformaldehyde, followed by decalcification in 10% EDTA solution for two weeks.

Subsequently, the decalcified femurs were embedded in paraffin and were sectioned into slices for TRAP staining. The images of staining slices were randomly obtained using a EVOS scanning microscope (Thermo Fisher Scientific, Waltham, MA, USA) at the same interested regions of each femur slice. Subsequently, the number of osteoclasts per bone perimeter (N.Oc/B.Pm) was quantified and osteoclast surface per bone surface (Oc.S/BS) was calculated to reflect OC formation within bone tissue slices.

**13. Statistical analysis**

All experiments were independently performed for at least three times. The value for each experiment were presented as mean ± standard deviation (SD). Student's t test was used to compare the difference between two groups, while for multigroup comparisons, the one-way ANOVA method was used. The GraphPad Prism (version 9.0) was used for all statistical analyses, and P value less than 0.05 were considered to be statistically significant.

**Results**

**1. The selective cytohesin inhibitor SecinH3 attenuates bone loss in OVX-induced osteoporosis model.**

To evaluate the effects of SecinH3 on OVX-induced bone loss, we constructed OVX models and treated mice with low (5 mg/kg) and high (10 mg/kg) doses of SecinH3. SecinH3 showed no significant damage to the kidney, heart, and liver at the two doses (Supplementary figure 1). Eight weeks after surgery, the trabecular bone in the OVX group decreased extensively compared to the sham group, while SecinH3 administration dose-dependently mitigated trabecular bone loss (figure 1A). ZA (0.05 mg/kg) was used as positive control and was also able to attenuate bone loss. Bone parameter analysis revealed that OVX decreased the BV/TV, Tb.N, Tb.Th, and mean density of bone volume by 68.5%, 21.8%, 28.9%, and 11.6%, respectively, while Tb.Sp was increased by 22.5%. These changes were all attenuated by SecinH3 at 5- and 10 mg/kg (figures 1B-F), similar to the effects of Zoledronic acid disodium. We

then measured the serum level of CTX-1, a specific marker of osteoclast resorptive activity, in mice of each group. Mice in the OVX group showed increased CTX-1, which was reduced by low and high doses of SecinH3 and ZA (0.05 mg/kg) treatment (figure 1G). Subsequent TRAP staining on femur bone slices indicated that the increased OCs in the OVX group were reduced by SecinH3 (figure 1H). N.OC/B.Pm and OC.S/BS were also lower in the low- and high-dose SecinH3-treated groups (figures 1I, J) than that in the OVX group. These results suggested SecinH3 can attenuate the osteoporotic phenotype induced by OVX.

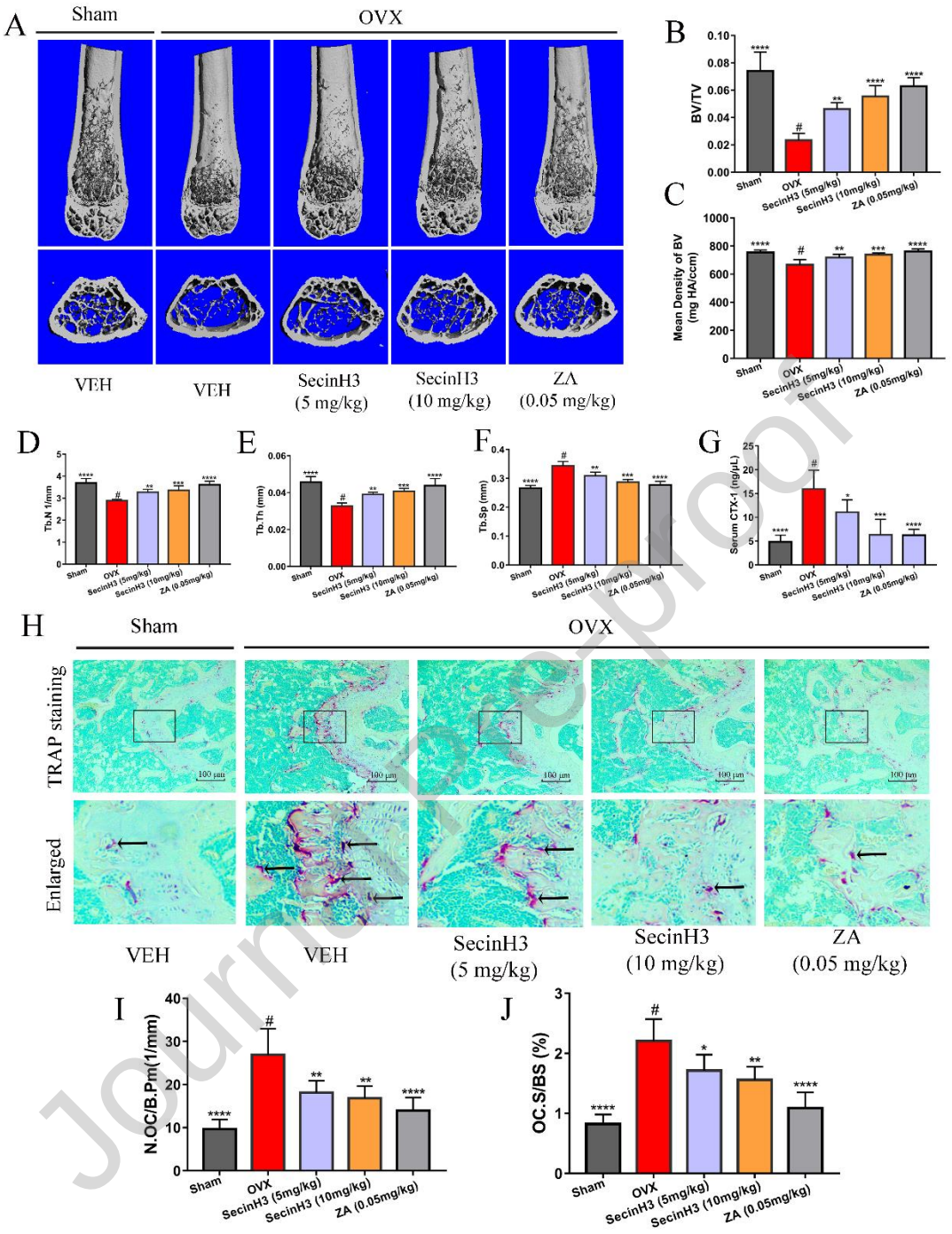


**Figure 1.**

**2. SecinH3 suppresses OC differentiation by inhibiting the function of cytohesin-2.**

We then examined the effects of SecinH3 on OC and osteoblast differentiation to determine how the compound attenuated bone loss in OVX mice. In vitro TRAP staining assay suggested that OC differentiation was dose-dependently inhibited by SecinH3 (figure 2A, B), without significant toxic effects on BMMs proliferation at the

indicated concentrations (figure 2C). The formation of OCs was completely abolished by 12 μM SecinH3. However, SecinH3 showed no effects on osteoblasts differentiation and mineralization (supplementary figure 2A, B). The expression of osteoblast specific genes, including *Runx2*, *Ocn*, and *Alp*, was also unchanged after SecinH3 (12 μM) treatment (supplementary figure 2C), suggesting that the anti-osteoporotic effects of SecinH3 depend on suppressing OC differentiation.

As SecinH3 is an effective inhibitor of cytohesin-1, cytohesin-2, and cytohesin-3 [20], we separately knocked down the three cytohesins by adeno-virus shRNA and induced OC differentiation to determine the responsible cytohesin for the effects of SecinH3. Western blot confirmed a knockdown efficiency of over 50% for each cytohesin, without affecting the other two cytohesins (figure 2 D, E). We then performed TRAP staining assay and found the differentiation of OC was impaired only by the knockdown of cytohesin-2, while cytohesin-1 and -3 showed no effects (figure 2 F, G), suggesting that SecinH3 exerts its effects on OC by inhibiting cytohesin-2. We then examined the the expression of cytohesin-2 during OC differentiation. However, we found the expression of cytohesin-2 on day 1, 3, and 5 after RANKL stimulation remained stable at both the mRNA and protein level (figure 2 H, I, J). This informed us that SecinH3 might affect cytohesin-2 mediated activation of ARF1 or ARF6 [15] to suppress OC differentiation.

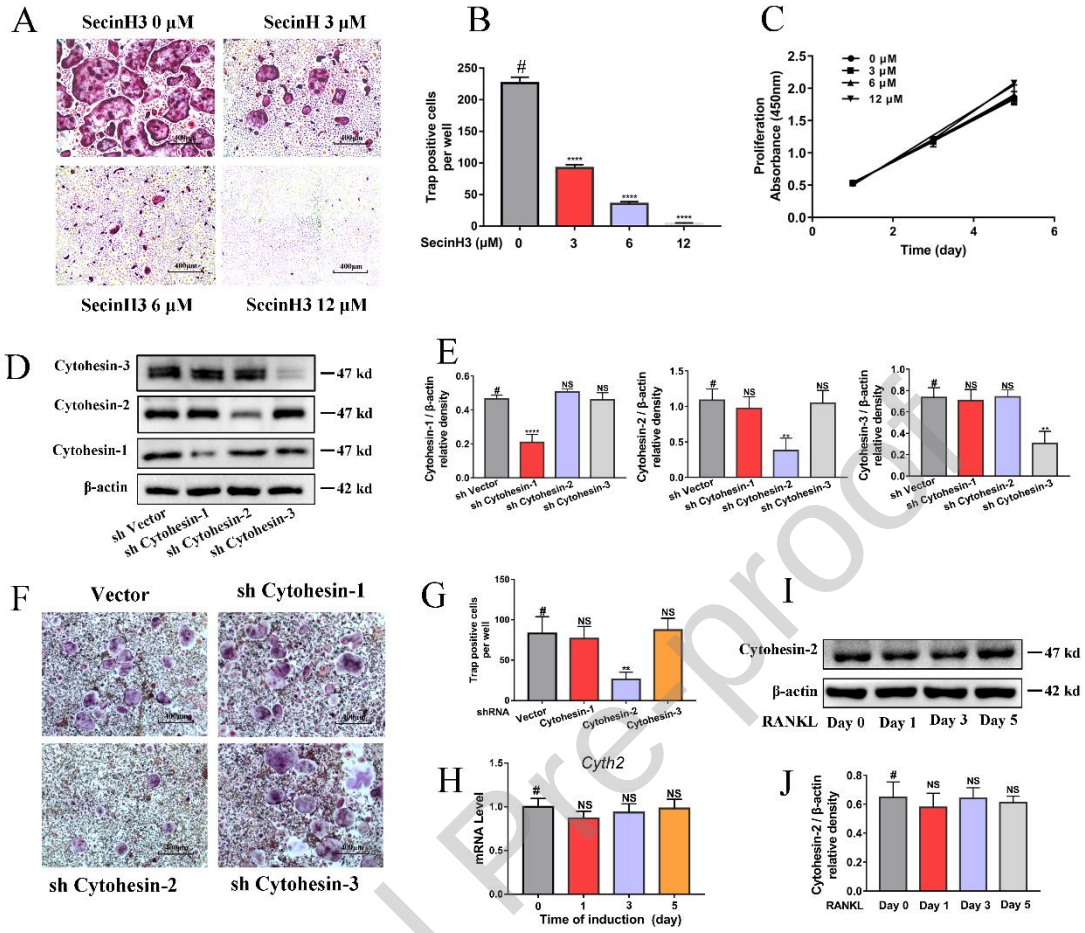


**Figure 2**

### 3. SecinH3 and cytohesin-2 silencing inhibit the activation of ARF1

To determine which ARF is responsible for the role of cytohesin-2 on OCs, we firstly examined the effects of NAV-2729, a selective inhibitor of ARF6, on OC differentiation. NAV-2729 specifically blocks cytohesin-2 mediated ARF6 activation, while having no effects on other ARFs, including ARF1 [24]. NAV-2729 had no effects on OC differentiation even at the maximal nontoxic concentration (figures 3A-C), indicating that ARF6 is not the downstream effector of cytohesin-2 in OCs. Then, we focused on ARF1. To determine the role of ARF1, we overexpressed both the dominant negative mutant ARF1 (T31N) and the constitutively GTP-restricted active ARF1 (Q71L) in BMMs (figure 3D-E) and induced OC differentiation. TRAP staining assay revealed more OCs differentiating from ARF1 (Q71L) overexpressing

BMMs and fewer OCs from ARF1 (T31N) overexpressing BMMs than the control group (figure 3F-G). Using a commercial ARF1 activation detecting kit, we found RANKL significantly induced ARF1 activation, which was suppressed after cytohesin-2 silencing (figure 3H-I) or SecinH3 treatment (figure 3J-K). Overexpression of ARF1 (Q71L) in BMMs was also able to rescue the inhibitory effects of SecinH3 on OC differentiation (figures 3L-M). In vivo, we found ARF1 was increased in BMMs from OVX mice, accompanied by increased OC specific proteins such as MMP9 and CTSK (figures 3N). These results suggested that SecinH3 suppresses OC differentiation via blocking cytohesin-2 mediated ARF1 activation.

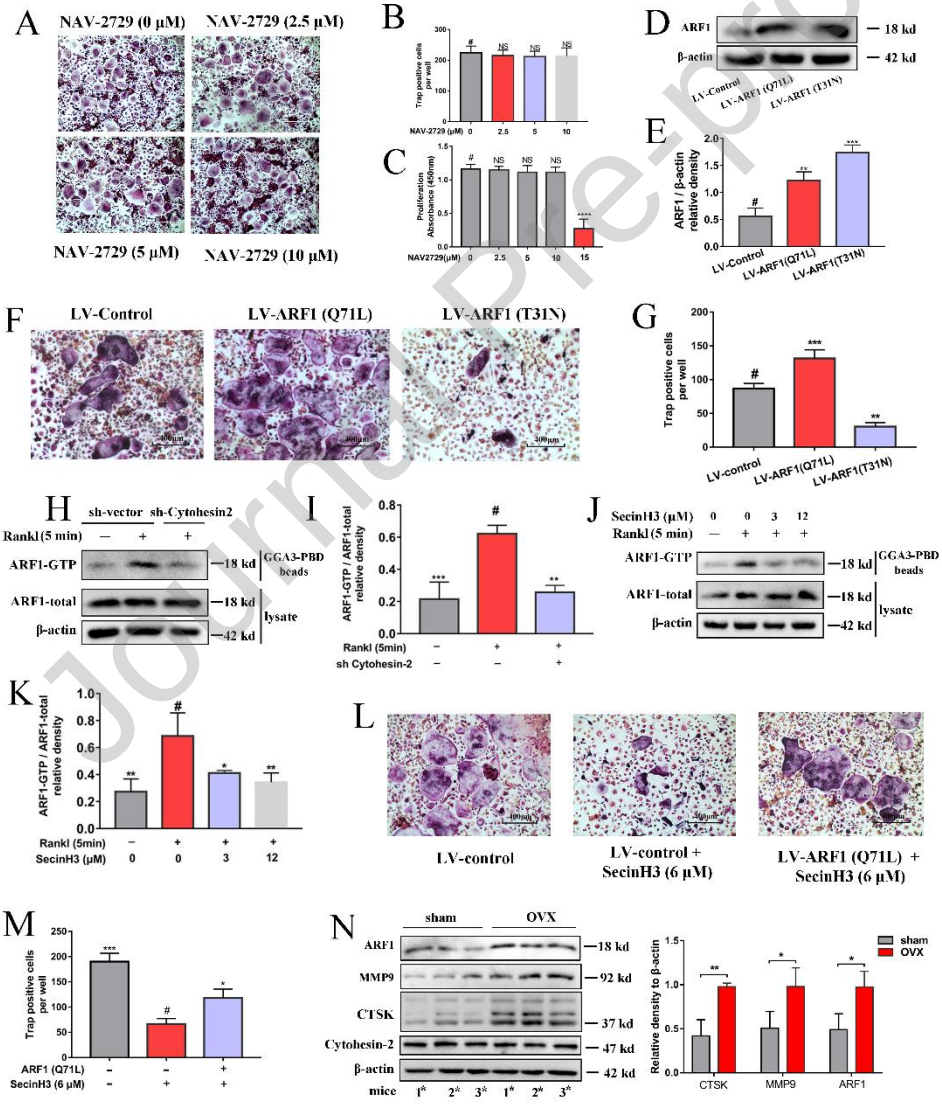


**Figure 3**

**4. SecinH3 or knockdown of cytohesin-2 reduces OC resorptive function.**

To perform the resorptive function, OCs adhere to the bone surface by forming actin rings and secrete $H^+$ and Cathepsin K (CTSK) into a local space within the actin rings, called sealing zone. The mRNA expression of *Ctsk* and other OC specific genes, such as *Mmp9*, *Nfatc1*, and *TRAP* was downregulated by SecinH3 in a dose-dependent manner (figure 4A). The protein level of these OC markers was also decreased by SecinH3 treatment on day 1, 3 and 5 during osteoclastogenesis (figure 4B). We then examined the effects of SecinH3 on the formation of podosome clusters and podosome belts, structures that dynamically form actin rings during OC differentiation. The results suggested that the number of podosome structures was significantly reduced by SecinH3 (figures 4C-D). Accordingly, less resorption pits were formed on the hydroxyapatite-coated culturing wells (figures 4E-F). SecinH3 administration at 12 μM almost abolished hydroxyapatite resorption by OCs. Similar results were observed after cytohesin-2 downregulation in OCs (figure 4G). Besides, the expression of CTSK, MMP9, NFATc1, and TRAP was also reduced after cytohesin-2 silencing (figures 4H-I). These results suggested that genetic downregulation or pharmacological inhibition of cytohesin-2 can reduce the resorptive function of OCs.

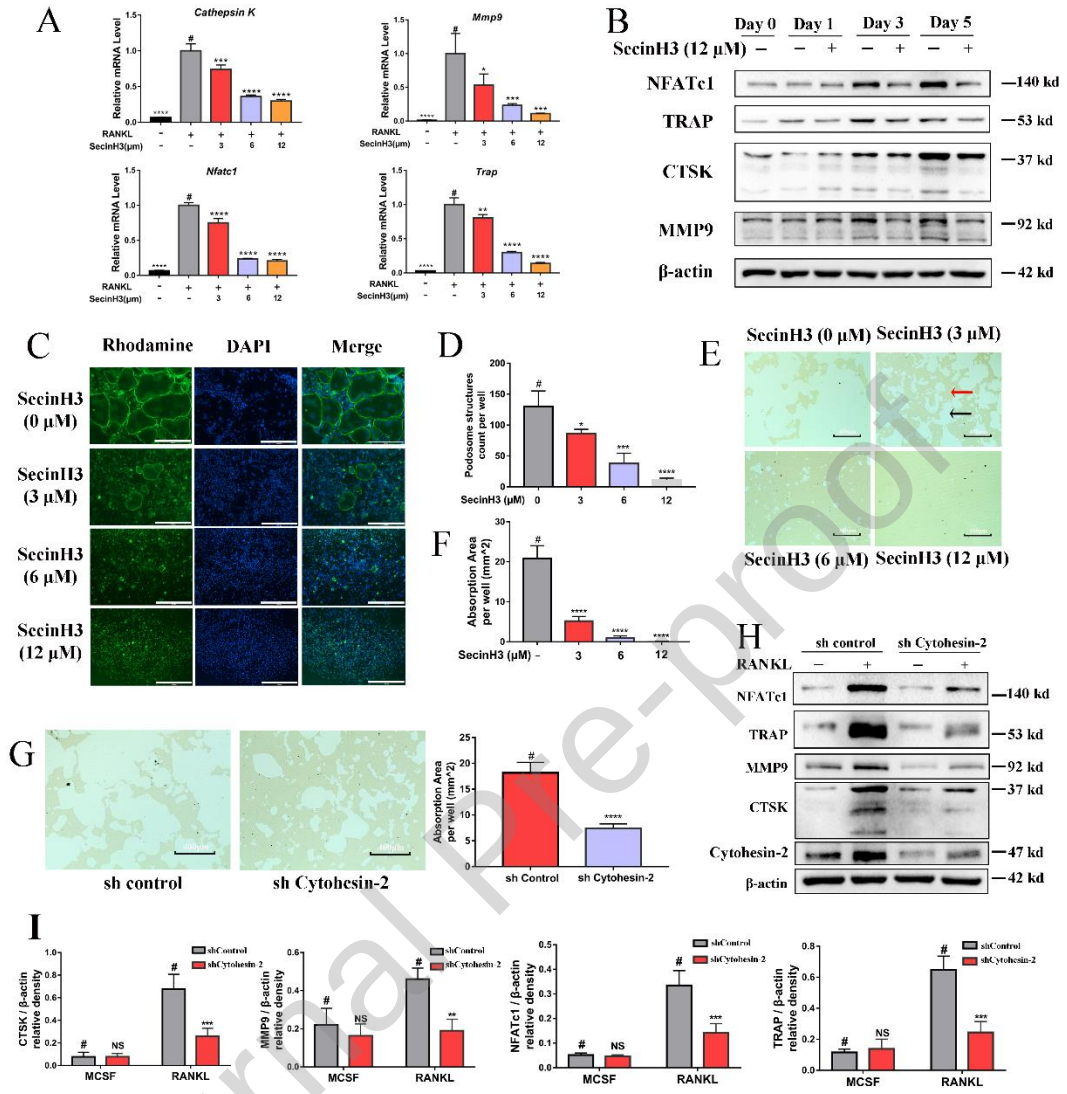


**Figure 4**

**5. Cytohesin-2 inhibition by SecinH3 inhibits the JNK pathway in the RANK signaling after RANKL treatment.**

To explore the mechanism by which SecinH3 inhibits OC, we performed RNA-sequencing on SecinH3 treated BMMs after RANKL stimulation. Principal component analysis on the sequencing data revealed different expression patterns between SecinH3 treated group and the control group (figure 5A). We then identified 447 upregulated and 1256 downregulated genes in the SecinH3-treated group by setting the threshold of $|\log_2(\text{Fold change})|$ to 0.5 (figure 5B) and the p-value to 0.01. Heatmaps revealed that the expression of OC maker genes, RANKL signaling

pathway related genes, and many inflammatory-related genes was all reduced by SecinH3 treatment (figure 5C). Accordingly, the KEGG analysis revealed that many inflammation-related pathways, such as TNF, IL-17, MAPK, and chemokine signaling pathway, were all significantly changed in the SecinH3 group (figure 5D). Of note, the MAPK signaling pathway had the most enriched genes, with the lowest p-value. Further differential analysis revealed that genes involved in this pathway were all downregulated by SecinH3 treatment (figure 5E). The GSEA analysis further confirmed the inhibition of the MAPK pathway in the SecinH3 group (figure 5F).

The MAPK pathway includes three main branches to transduce OC differentiation signaling: the JNK, ERK and p38 pathways. To determine which pathway is responsible for the effects of SecinH3, we performed Western blot assays to examine the changes of the three pathways at 15, 30 and 60 minutes after RANKL treatment. We found the activation of p-JNK was inhibited by 64%, 48%, and 43% at 15, 30 and 60 min, respectively (figures 5G-H). These inhibition rates were more significant than that on p-p38 (26%, 41%, and 31% at 15, 30, and 60 min, respectively). The ERK pathway was not affected by SecinH3 treatment (figures 5G-H). These results demonstrated that JNK pathway is the main downstream pathway responsible for the effects of SecinH3. We then transinfected BMMs with cytohesin-2 shRNA adenovirus, and found that cytohesin-2 silencing also significantly suppressed the activation of JNK (figures 5I-J), indicating that the JNK pathway is responsible for cytohesin-2 induced OC differentiation.

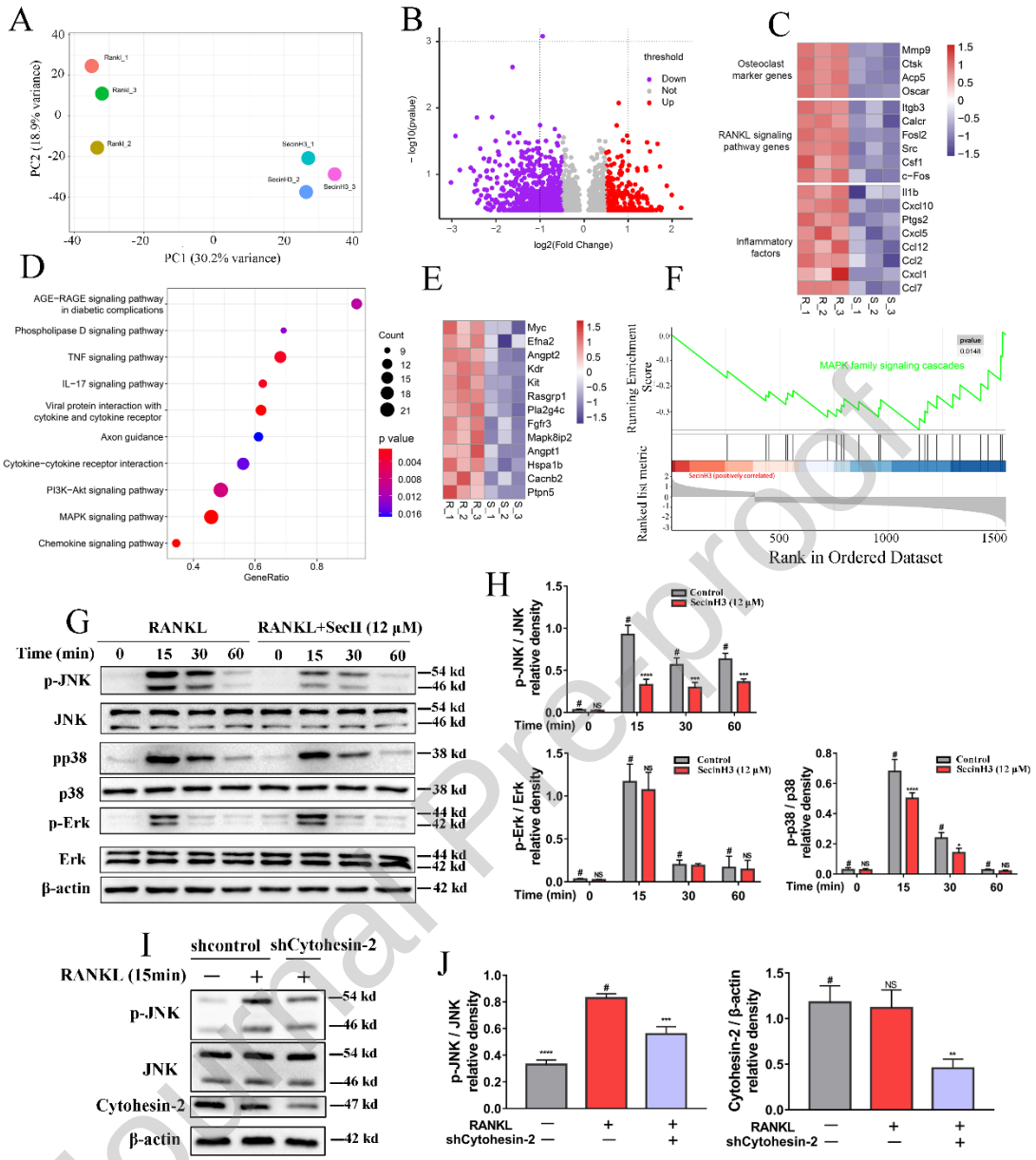


**Figure 5**

**6. Cytohesin-2 inhibition reduces the endoribonuclease activity of IRE1 and the UPR process.**

Previously, we have revealed the PERK branch of the UPR is involved in osteoclast differentiation and function [9]. The JNK pathway is also associated with the activity of IRE1 [10], which mediates the UPR of ER stress. Considering the effects of cytohesin-2 on JNK, we speculated that there might be an association between cytohesin-2 and the IRE1 mediated UPR. To confirm this hypothesis, we used a pair

of specific primers to detect the mRNA level of *XBP1s* [25], which is the specific product of the endoribonuclease activity of IRE1 during UPR [11, 12]. The results showed that the mRNA level of *XBP1s* was increased in a time-dependent manner after RANKL treatment, but was decreased by SecinH3 after 8 and 16 hours of RANKL treatment (figure 6A). The endoribonuclease activity of IRE1 is augmented by its autophosphorylation (p-IRE1) [11, 12]. Western blot analysis revealed both p-IRE1 and XBP1s were inhibited by 12 μM SecinH3 (figures 6B-C) or by cytohesin-2 silencing (figure 6D). On the contrary, when ARF1(Q71L) was overexpressed in BMMs, SecinH3 mediated inhibition of p-IRE1 and XBP1s was reversed (figure 6E). Subsequently, we used thapsigargin (TG), a well-known p-IRE1 and ER stress inducer [26], to confirm the role of p-IRE1 in SecinH3-mediated OC inhibition. TG at 0.1 nM significantly promoted OC differentiation and attenuated the inhibition of OC formation due to SecinH3 (figures 6F-G) or cytohesin-2 silencing (figures 6H-I). TG also recovered the resorptive function of OCs treated with SecinH3 (figure 6J), and the expression of NFATc1, TRAP, MMP9 and CTSK was increased by TG compared to the SecinH3 group (figures 6K-L). These results suggested that the cytohesin-2/ARF1 axis promotes OC differentiation by regulating the endoribonuclease activity of IRE1.

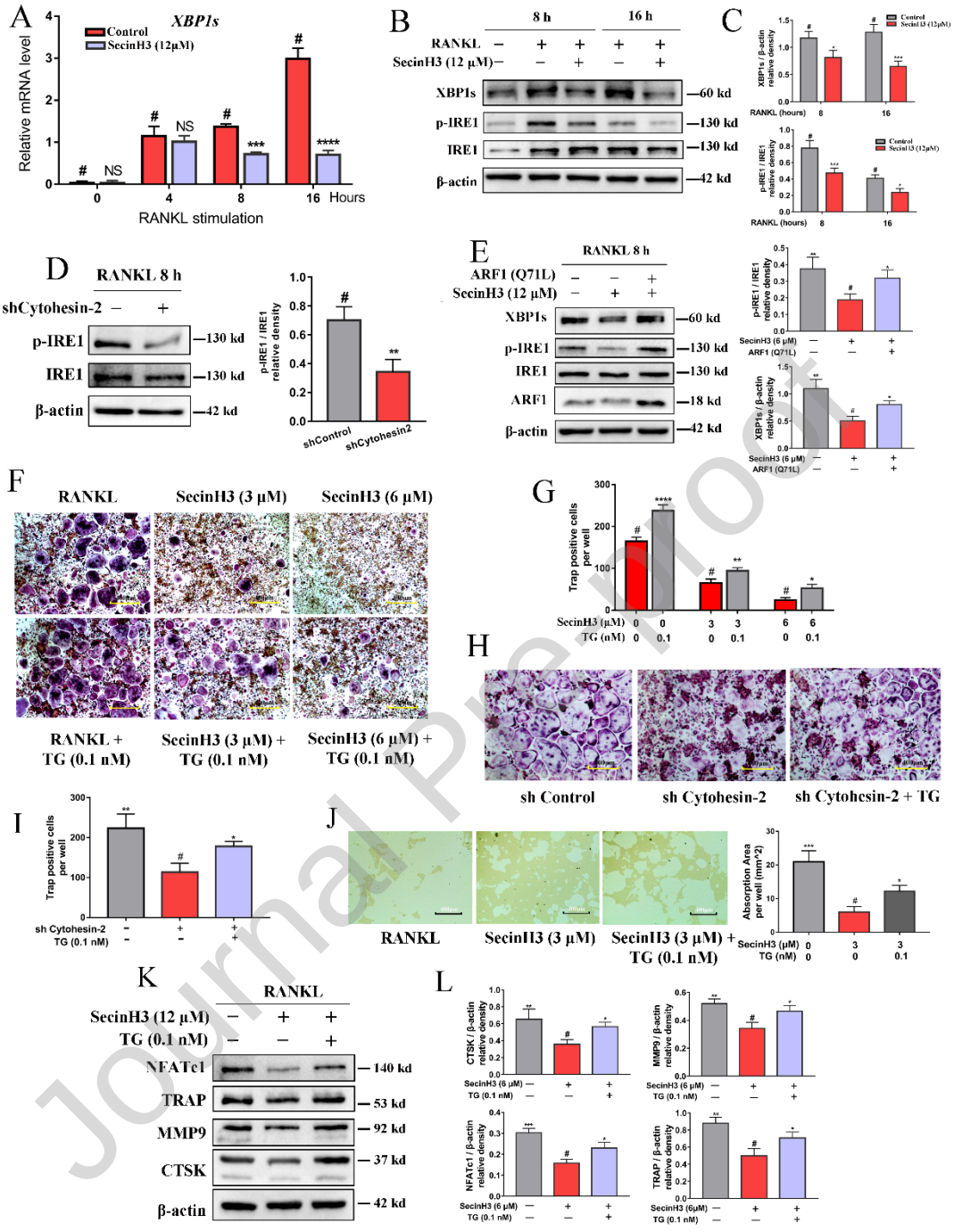


**Figure 6**

**7. The JNK pathway acts upstream to control the endoribonuclease activity of IRE1.**

IRE1 possesses both kinase and endoribonuclease activities. It is well established that JNK can be activated by the kinase activity of IRE1 [10], while the association

between JNK and the endoribonuclease activity of IRE1 has not been reported. In this study, we observed that the JNK pathway was activated early at 15min after RANKL stimulation (Figure 5G), while p-IRE1 and XBP1s, which reflect the endoribonuclease activity of IRE1, were observed to be significant 8 hours after RANKL treatment (Figure 6B). This led us to question the up and downstream relationships between the two pathways, which were all regulated by cytohesin-2 and suppressed by its inhibitor SecinH3. Firstly, we found OC differentiation was suppressed by either the JNK pathway inhibitor SP600125 (10 μM), or the IRE1 endoribonuclease activity inhibitor 4μ8C (5 μM) (figures 7A-B). IRE1 inhibitor 4μ8C had no influence on p-JNK level 15 minutes after RANKL treatment (figure 7C). Eight hours after RANKL treatment, we were unable to detect p-JNK level by western blot, indicating that the IRE1 endoribonuclease activity has no effect on the activation of JNK. Then, we found that the p-IRE1 was significantly inhibited by the JNK inhibitor SP600125 15 minutes and 8 hours after RANKL stimulation (figures 7D-E). Further, we found OC inhibition could be rescued by inducing p-IRE1 activation with TG in BMMs treated with SP600125 (figure 7F). These findings suggested that the JNK pathway is regulated by the cytohesin-2/ARF1 axis following RANKL stimulation and acts upstream to mediate the endoribonuclease activity of IRE1, which further promotes osteoclastogenesis (figure 8).

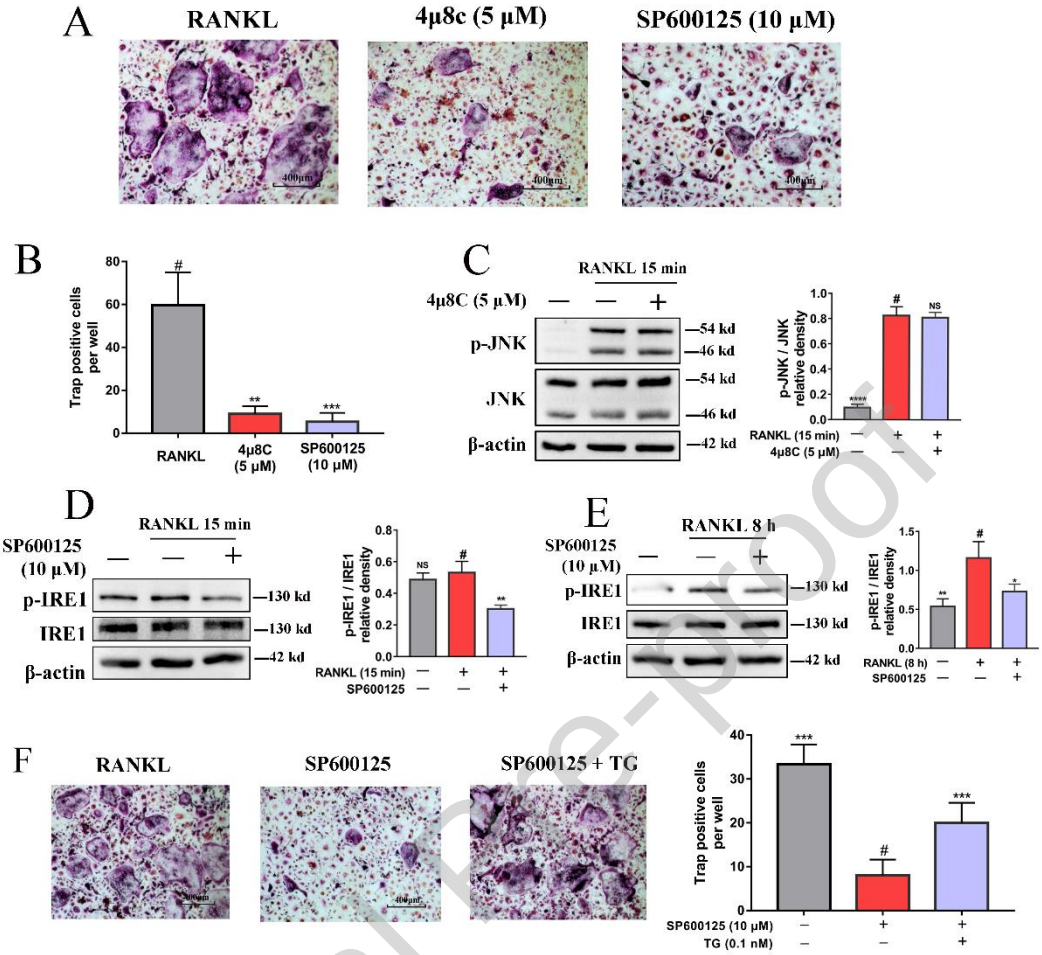


**Figure 7**

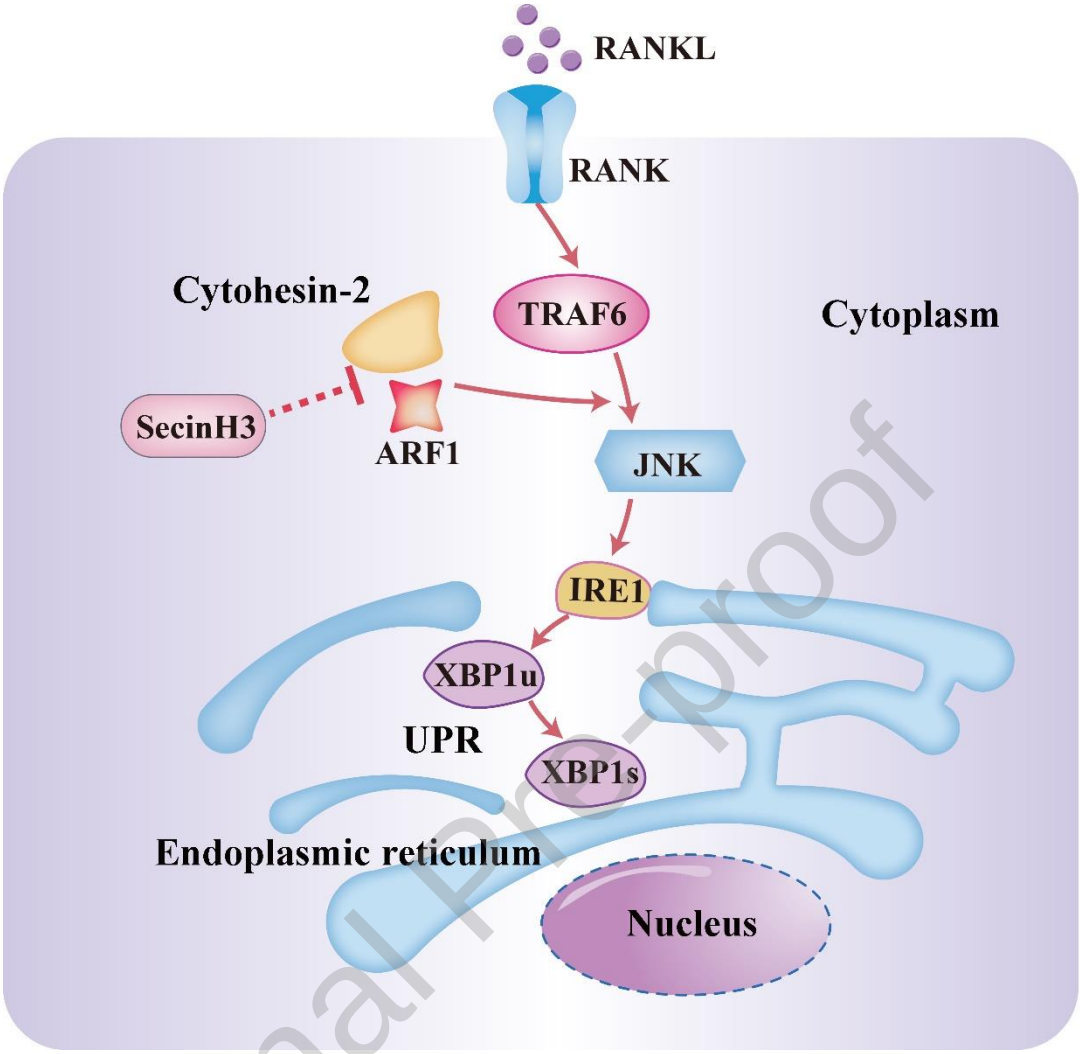


**Figure 8**



**Discussion**

In this study, we found the cytohesin-2/ARF1 axis is involved in OC differentiation and resorptive function. Both genetic knockdown or pharmacological inhibition of cytohesin-2 suppressed OC formation and function, and in vivo administration of SecinH3 attenuated bone loss induced by OVX in mice. RNA-sequencing revealed that the JNK pathway was suppressed by cythohesin-2 inhibition. We further found the JNK pathway can regulate the endoribonuclease activity of IRE1 and promoted XBP1 splicing. Suppressing the cytohesin-2/ARF1/JNK/p-IRE1 pathway by SecinH3 might be a potential strategy for the treatment of osteoporosis.

Among the four cytohesins, cytohesin-2 has attracted more attention due to its involvement in various biological processes, such as podosome assembly [27], protein recycling [28], signal transduction [18], and cell migration [29, 30]. Cytohesin-2 is also important for neuron dendritic formation [31], neurite growth [32], nerve myelination [33], and is involved in motor neuron disease [34]. In most cases, cytohesin-2 performs its function via activating either ARF1 or ARF6 [15]. For example, cytohesin-2 is involved in the TLR-2 and IL-1β signaling by binding to the adaptor MYD88 [18, 35]. In these two pathways, cytohesin-2 activates ARF6 to contribute to the downstream signaling transduction. In this study, we found cytohesin-2 activates ARF1, other than ARF6, to transduce the RANK signaling to JNK and promotes OC differentiation.

We precluded the role ARF6 as a downstream effector of cytohesin-2 in OCs by using the selective ARF6 inhibitor NAV-2729. A previous study has shown that NAV-2729 is a dual inhibitor of both ARF1 and ARF6 [36], but the activation of ARF1 in the article is triggered by BRAG2, other than the cytohesin proteins. BRAG2 belongs to another kind of guanine nucleotide exchange factor to activate the ARF proteins [37]. In the initial study discovering NAV-2729, the compound demonstrated high selectivity and targeted only ARF6 after cytohesin-2 treatment, but showed no effects on the activation of other ARFs, including ARF1 [24], indicating that NAV-2729 serves as a specific inhibitor of cytohesin-2 mediated ARF6 mediation. In this study, we found NAV-2729 did not affect the differentiation of OC, concluding that ARF6 is less likely to act as a downstream effector of cythoesin-2 during OC differentiation. This result is consistent with a previous finding that ARF6 negatively regulates the function of OCs by impairing the assembly of sealing zones, which are core structures for the bone resorptive function of OCs [38]. We then confirmed the role of ARF1 because the inhibition of OC differentiation by SecinH3 was attenuated by the over-expression of ARF1 (Q71L). A previous study found that ARF1 is involved in OC proliferation, migration and differentiation [19]. In this study, we found

cytohesin-2 is the key GEF to activate ARF1 after RANKL treatment.

During differentiation, OC precursors and OCs are highly active in protein synthesis, which increases the accumulation of unfolded proteins in the ER and requires the UPR to eliminate these proteins. The role of UPR during OC differentiation has been well evaluated. For example, a previous study showed that the PERK branch of the UPR is activated after 1-3 days of RANKL stimulation [9]. Another study suggested the activity of IRE1/XBP1s branch increases with time and peaks two days after RANKL treatment [8]. The level of p-IRE1 can be activated as early as 3 hours after RANKL treatment in RAW264.7 cells [39]. In this study, we also observed that p-IRE1 level was significantly increased 8 hours after RANKL stimulation, compared to the un-induced group. These results convergently evidenced that the p-IRE1 mediated UPR is essential for OC differentiation. However, how the RANK signaling is transduced to p-IRE1 and activates the UPR has never been explored in previous studies.

In this study, we found the JNK pathway can regulate the p-IRE1/XBP1s branch of UPR after RANKL treatment. We arrived to this result by the sequential activation of the JNK and IRE-1 after RANKL stimulation. Following RANKL treatment, p-IRE1 was activated at least after eight hours, while p-JNK was transiently activated as early as 15 minutes, and was almost undetectable 8 hours after RNAKL treatment, suggesting that JNK is activated earlier in the RANK signaling than p-IRE1. Subsequently, we found p-IRE1 was significantly inhibited by the JNK inhibitor SP600125, while 4μ8C, the selective inhibitor on the endoribonuclease activity of IRE1, had no significant effects on transient p-JNK activation. These results suggested that JNK acts upstream to regulate the endoribonuclease activity of IRE1 in the RANK signaling, which adds novel understanding to the well-established knowledge that IRE1 acts upstream via its protein kinase activity to activate the JNK pathway [10, 40].

Finally, we found the RANK-JNK-IRE1 pathway is regulated by the cytohesin-2/ ARF1 axis. Targeting the axis by SecinH3 or by cytoheisn-2 knockdown inhibited the activation of both JNK and IRE1 and suppressed OC differentiation. In vivo treatment with SecinH3 also attenuated bone loss after OVX, similar to the effects of ZA, suggesting that the cytohesin-2/ARF1 axis might be a potential target for the treatment of post-menopause osteoporosis. Currently, bisphosphonates are widely used for the treatment of post-menopause osteoporosis due to their potent anti-osteoclast effects. However, patient compliance to bisphosphonate therapy is poor due to fear of severe adverse effects associated with these drugs. Other drugs, such as teriparatide and denosumab, are more effective than bisphosphonates in preventing osteoporosis-related fractures, but the higher cost also increases the economic burden, especially for patients from low-income countries [1]. Thus, developing new drugs that are therapeutically efficient and cost effective will help benefit more patients with osteoporosis. In this study, the ctyohesin-2 inhibitor SecinH3 was safe for in vivo administration and showed similar anti-osteoporosis effects in OVX models, indicating that this agent may be an alternative option for the treatment of osteoporosis. Future clinical studies are in need to evaluate the safety and efficacy to treat osteoporosis in human subjects.

**Conclusions**

Conclusively, our results showed that the cytohesin-2/ARF1 axis is involved in the RANK signaling and OC differentiation. Genetic knockdown or pharmacological inhibition of cytoheisn-2 by SecinH3 inhibits OC differentiation and function. SecinH3 can also ameliorate OVX-induced bone loss in vivo. Mechanistically, cytohesin-2 and ARF1 activates the JNK pathway in the RANK signaling, which further regulates the endoribonuclease activity of IRE1 and promotes the IRE1/XBP1s branch of UPR, leading to the facilitation of osteoclast differentiation. Disrupting the cytohesin-2/ARF1/JNK/p-IRE1 pathway by SecinH3 might be a potential strategy for the treatment of osteoporosis and related clinical studies are in need to further confirm the therapeutic value of the agent.

**Conflict of interest**

The authors have declared that no conflict of interest exists.

**Acknowledgements**

We appreciate the National Natural Science Foundation of China for the grants (no. 82072500, 82002354) in the supporting of this work.

**Author contributions**

FL and HFG conceived and supervised the study. YMD and KHS designed the experiments. YMD, KHS performed the experiments and analyzed the data. YMD wrote the manuscript and prepared the figure. XT drew the graphical abstract. PJW, JCG, HLK, RPP, MPZ, KXY and QG, and XW participated in the experiments and were responsible for technical, or material support.

## References

[1] Y. Dong, R. Peng, H. Kang, K. Song, Q. Guo, H. Zhao, M. Zhu, Y. Zhang, H. Guan, F. Li, Global incidence, prevalence, and disability of vertebral fractures: a systematic analysis of the global burden of disease study 2019, Spine J 22(5) (2022) 857-868.
[2] Y. Dong, H. Kang, R. Peng, K. Song, Q. Guo, H. Guan, M. Zhu, D. Ye, F. Li, Global, regional, and national burden of low bone mineral density from 1990 to 2019: results from the Global Burden of Disease Study 2019, Front. Endocrinol. (Lausanne) 13 (2022) 870905.
[3] J.E. Compston, M.R. McClung, W.D. Leslie, Osteoporosis, Lancet 393(10169) (2019) 364-376.
[4] J.M. Kim, C. Lin, Z. Stavre, M.B. Greenblatt, J.H. Shim, Osteoblast-Osteoclast Communication and Bone Homeostasis, Cells 9(9) (2020).
[5] J.H. Park, N.K. Lee, S.Y. Lee, Current Understanding of RANK Signaling in Osteoclast Differentiation and Maturation, Mol. Cells 40(10) (2017) 706-713.
[6] K. Kim, S.H. Lee, J. Ha Kim, Y. Choi, N. Kim, NFATc1 induces osteoclast fusion via up-regulation of Atp6v0d2 and the dendritic cell-specific transmembrane protein (DC-STAMP), Mol. Endocrinol. 22(1) (2008) 176-85.
[7] W.J. Boyle, W.S. Simonet, D.L. Lacey, Osteoclast differentiation and activation, Nature 423(6937) (2003) 337-42.
[8] T. Tohmonda, M. Yoda, T. Iwawaki, M. Matsumoto, M. Nakamura, K. Mikoshiba, Y. Toyama, K. Horiuchi, IRE1alpha/XBP1-mediated branch of the unfolded protein response regulates osteoclastogenesis, J. Clin. Invest. 125(8) (2015) 3269-79.

[9] J. Guo, R. Ren, K. Sun, X. Yao, J. Lin, G. Wang, Z. Guo, T. Xu, F. Guo, PERK controls bone homeostasis through the regulation of osteoclast differentiation and function, Cell Death Dis. 11(10) (2020) 847.
[10] F. Urano, X. Wang, A. Bertolotti, Y. Zhang, P. Chung, H.P. Harding, D. Ron, Coupling of stress in the ER to activation of JNK protein kinases by transmembrane protein kinase IRE1, Science 287(5453) (2000) 664-6.
[11] T.K. Chang, D.A. Lawrence, M. Lu, J. Tan, J.M. Harnoss, S.A. Marsters, P. Liu, W. Sandoval, S.E. Martin, A. Ashkenazi, Coordination between Two Branches of the Unfolded Protein Response Determines Apoptotic Cell Fate, Mol. Cell 71(4) (2018) 629-636 e5.
[12] S. Bashir, M. Banday, O. Qadri, A. Bashir, N. Hilal, I.F. Nida, S. Rader, K.M. Fazili, The molecular mechanism and functional diversity of UPR signaling sensor IRE1, Life Sci. 265 (2021) 118740.
[13] J. Wang, Z. Fang, C. Song, H. Kang, Q. Guo, Y. Dong, Y. Zhang, R. Peng, H. Guan, F. Li, Schisandrin B Inhibits Osteoclastogenesis and Protects Against Ovariectomy-Induced Bone Loss, Front. Pharmacol. 11 (2020) 1175.
[14] Q. Guo, H. Kang, J. Wang, Y. Dong, R. Peng, H. Zhao, W. Wu, H. Guan, F. Li, Inhibition of ACLY Leads to Suppression of Osteoclast Differentiation and Function Via Regulation of Histone Acetylation, J. Bone Miner. Res. 36(10) (2021) 2065-2080.
[15] W. Kolanus, Guanine nucleotide exchange factors of the cytohesin family and their roles in signal transduction, Immunol. Rev. 218 (2007) 102-13.
[16] B. Fuss, T. Becker, I. Zinke, M. Hoch, The cytohesin Steppke is essential for insulin signalling in Drosophila, Nature 444(7121) (2006) 945-8.
[17] A. Hurtado-Lorenzo, M. Skinner, J. El Annan, M. Futai, G.H. Sun-Wada, S. Bourgoin, J. Casanova, A. Wildeman, S. Bechoua, D.A. Ausiello, D. Brown, V. Marshansky, V-ATPase interacts with ARNO and Arf6 in early endosomes and regulates the protein degradative pathway, Nat. Cell Biol. 8(2) (2006) 124-36.
[18] W. Zhu, N.R. London, C.C. Gibson, C.T. Davis, Z. Tong, L.K. Sorensen, D.S. Shi, J. Guo, M.C. Smith, A.H. Grossmann, K.R. Thomas, D.Y. Li, Interleukin receptor activates a MYD88-ARNO-ARF6 cascade to disrupt vascular stability, Nature 492(7428) (2012) 252-5.
[19] M.J. Kim, H. Kim, S.H. Lee, D.R. Gu, S.Y. Lee, K. Lee, D. Jeong, ADP-Ribosylation Factor 1 Regulates Proliferation, Migration, and Fusion in Early Stage of Osteoclast Differentiation, Int. J. Mol. Sci. 16(12) (2015) 29305-14.
[20] M. Hafner, A. Schmitz, I. Grune, S.G. Srivatsan, B. Paul, W. Kolanus, T. Quast, E. Kremmer, I. Bauer, M. Famulok, Inhibition of cytohesins by SecinH3 leads to hepatic insulin resistance, Nature 444(7121) (2006) 941-4.
[21] J.C. Norman, D. Jones, S.T. Barry, M.R. Holt, S. Cockcroft, D.R. Critchley, ARF1 mediates paxillin recruitment to focal adhesions and potentiates Rho-stimulated stress fiber formation in intact and permeabilized Swiss 3T3 fibroblasts, J. Cell Biol. 143(7) (1998) 1981-95.
[22] H.Y. Yoon, J.S. Bonifacino, P.A. Randazzo, In vitro assays of Arf1 interaction with GGA proteins, Methods Enzymol. 404 (2005) 316-32.
[23] S. Pozzi, S. Vallet, S. Mukherjee, D. Cirstea, N. Vaghela, L. Santo, E. Rosen, H.

Ikeda, Y. Okawa, T. Kiziltepe, J. Schoonmaker, W. Xie, T. Hideshima, E. Weller, M.L. Bouxsein, N.C. Munshi, K.C. Anderson, N. Raje, High-dose zoledronic acid impacts bone remodeling with effects on osteoblastic lineage and bone mechanical properties, Clin. Cancer Res. 15(18) (2009) 5829-39.
[24] J.H. Yoo, D.S. Shi, A.H. Grossmann, L.K. Sorensen, Z. Tong, T.M. Mleynek, A. Rogers, W. Zhu, J.R. Richards, J.M. Winter, J. Zhu, C. Dunn, A. Bajji, M. Shenderovich, A.L. Mueller, S.E. Woodman, J.W. Harbour, K.R. Thomas, S.J. Odelberg, K. Ostanin, D.Y. Li, ARF6 Is an Actionable Node that Orchestrates Oncogenic GNAQ Signaling in Uveal Melanoma, Cancer Cell 29(6) (2016) 889-904.
[25] S.B. Yoon, Y.H. Park, S.A. Choi, H.J. Yang, P.S. Jeong, J.J. Cha, S. Lee, S.H. Lee, J.H. Lee, B.W. Sim, B.S. Koo, S.J. Park, Y. Lee, Y.H. Kim, J.J. Hong, J.S. Kim, Y.B. Jin, J.W. Huh, S.R. Lee, B.S. Song, S.U. Kim, Real-time PCR quantification of spliced X-box binding protein 1 (XBP1) using a universal primer method, PLoS One 14(7) (2019) e0219978.
[26] H. Lee, J.Y. Noh, Y. Oh, Y. Kim, J.W. Chang, C.W. Chung, S.T. Lee, M. Kim, H. Ryu, Y.K. Jung, IRE1 plays an essential role in ER stress-mediated aggregation of mutant huntingtin via the inhibition of autophagy flux, Hum. Mol. Genet. 21(1) (2012) 101-14.
[27] N.B. Rafiq, Z.Z. Lieu, T. Jiang, C.H. Yu, P. Matsudaira, G.E. Jones, A.D. Bershadsky, Podosome assembly is controlled by the GTPase ARF1 and its nucleotide exchange factor ARNO, J. Cell Biol. 216(1) (2017) 181-197.
[28] J.C. Salem, M.M. Reviriego-Mendoza, L.C. Santy, ARF-GEF cytohesin-2/ARNO regulates R-Ras and alpha5-integrin recycling through an EHD1-positive compartment, Mol. Biol. Cell 26(23) (2015) 4265-79.
[29] S. Lee, J.G. Wurtzel, L.E. Goldfinger, The RLIP76 N-terminus binds ARNO to regulate PI 3-kinase, Arf6 and Rac signaling, cell spreading and migration, Biochem. Biophys. Res. Commun. 454(4) (2014) 560-5.
[30] J.C. Davies, S. Tamaddon-Jahromi, R. Jannoo, V. Kanamarlapudi, Cytohesin 2/ARF6 regulates preadipocyte migration through the activation of ERK1/2, Biochem. Pharmacol. 92(4) (2014) 651-60.
[31] A. Ito, M. Fukaya, S. Saegusa, E. Kobayashi, T. Sugawara, Y. Hara, J. Yamauchi, H. Okamoto, H. Sakagami, Pallidin is a novel interacting protein for cytohesin-2 and regulates the early endosomal pathway and dendritic formation in neurons, J. Neurochem. 147(2) (2018) 153-177.
[32] T. Torii, Y. Miyamoto, K. Tago, K. Sango, K. Nakamura, A. Sanbe, A. Tanoue, J. Yamauchi, Arf6 guanine nucleotide exchange factor cytohesin-2 binds to CCDC120 and is transported along neurites to mediate neurite growth, J. Biol. Chem. 289(49) (2014) 33887-903.
[33] T. Torii, N. Ohno, Y. Miyamoto, K. Kawahara, Y. Saitoh, K. Nakamura, S. Takashima, H. Sakagami, A. Tanoue, J. Yamauchi, Arf6 guanine-nucleotide exchange factor cytohesin-2 regulates myelination in nerves, Biochem. Biophys. Res. Commun. 460(3) (2015) 819-25.
[34] J. Zhai, L. Zhang, J. Mojsilovic-Petrovic, X. Jian, J. Thomas, K. Homma, A. Schmitz, M. Famulok, H. Ichijo, Y. Argon, P.A. Randazzo, R.G. Kalb, Inhibition of

Cytohesins Protects against Genetic Models of Motor Neuron Disease, J. Neurosci. 35(24) (2015) 9088-105.
[35] Y. Duan, R. Prasad, D. Feng, E. Beli, S. Li Calzi, A.L.F. Longhini, R. Lamendella, J.L. Floyd, M. Dupont, S.K. Noothi, G. Sreejit, B. Athmanathan, J. Wright, A.R. Jensen, G.Y. Oudit, T.A. Markel, P.R. Nagareddy, A.G. Obukhov, M.B. Grant, Bone Marrow-Derived Cells Restore Functional Integrity of the Gut Epithelial and Vascular Barriers in a Model of Diabetes and ACE2 Deficiency, Circ. Res. 125(11) (2019) 969-988.
[36] S. Benabdi, F. Peurois, A. Nawrotek, J. Chikireddy, T. Caneque, T. Yamori, I. Shiina, Y. Ohashi, S. Dan, R. Rodriguez, J. Cherfils, M. Zeghouf, Family-wide Analysis of the Inhibition of Arf Guanine Nucleotide Exchange Factors with Small Molecules: Evidence of Unique Inhibitory Profiles, Biochemistry 56(38) (2017) 5125-5133.
[37] D. Karandur, A. Nawrotek, J. Kuriyan, J. Cherfils, Multiple interactions between an Arf/GEF complex and charged lipids determine activation kinetics on the membrane, Proc. Natl. Acad. Sci. U. S. A. 114(43) (2017) 11416-11421.
[38] T. Heckel, C. Czupalla, A.I. Expirto Santo, M. Anitei, M. Arantzazu Sanchez-Fernandez, K. Mosch, E. Krause, B. Hoflack, Src-dependent repression of ARF6 is required to maintain podosome-rich sealing zones in bone-digesting osteoclasts, Proc. Natl. Acad. Sci. U. S. A. 106(5) (2009) 1451-6.
[39] L. Raimondi, A. De Luca, S. Fontana, N. Amodio, V. Costa, V. Carina, D. Bellavia, S. Raimondo, S. Siragusa, F. Monteleone, R. Alessandro, M. Fini, G. Giavaresi, Multiple Myeloma-Derived Extracellular Vesicles Induce Osteoclastogenesis through the Activation of the XBP1/IRE1alpha Axis, Cancers (Basel) 12(8) (2020).
[40] H. Kato, S. Nakajima, Y. Saito, S. Takahashi, R. Katoh, M. Kitamura, mTORC1 serves ER stress-triggered apoptosis via selective activation of the IRE1-JNK pathway, Cell Death Differ. 19(2) (2012) 310-20.

**Figure 1. The selective cytohesin inhibitor SecinH3 attenuates bone loss in OVX-induced osteoporosis models.** (A) Representative 3D-constructed images of the distal femurs of mice in each group. Zoledronic Acid disodium tetrahydrate (ZA, 0.05 mg/kg) was used as positive control. (B-F) The morphometric parameters of trabeculae bone, including bone volume/tissue volume (BV/TV), mean density of bone volume (mg HA/ccm), trabecular numbers (Tb.N), trabecular thickness (Tb.Th), and trabecular space (Tb.Sp). (G) The serum concentration of C-terminal telopeptide of type I collagen (CTX-1) in each group. (H) Representative images and the enlarged areas of the TRAP staining on femur slices for each group. Scale bar was indicated within each image. (I, J) The number of osteoclasts per bone perimeter (N.Oc/B.Pm) and osteoclast surface per bone surface (Oc.S/BS) of TRAP staining to reflect the formation of mature OCs on bone tissue slices. Abbreviations: VEH, vehicle; OVX, ovariectomy; Statistical significance: * $P < 0.05$; ** $P < 0.01$; *** $P < 0.001$; **** $P < 0.0001$. "#" indicates the control group in each comparison.

**Figure 2. SecinH3 suppresses OC differentiation by inhibiting cytohesin-2.** (A, B) Dose-dependent inhibition on OC differentiation by SecinH3; scale bar, 400 μm. (C) CCK8 assay precluded the cytotoxicity of SecinH3 on BMM proliferation at indicated concentrations. The assays were performed on day 1, 3, and 5 of culturing. (D, E) Knockdown efficacy of adenovirus-shRNA targeting cytohesin-1, -2, and -3, respectively. (F, G) OC differentiation after knockdown of cytohesin-1, -2 or -3, respectively; scale bar, 400 μm. (H) The mRNA level of cytohesin-2 after 1, 3 and 5 days of RANKL treatment. (I, J) The expression of cytoheisn-2 at the protein level on day 1, 3, and 5 during OC differentiation. Statistical significance: * $P < 0.05$; ** $P < 0.01$; *** $P < 0.001$; **** $P < 0.0001$; NS, no significance. "#" indicates the control group in each comparison.

**Figure 3. SecinH3 and cytohesin-2 silencing inhibit the activation of ARF1 after RANKL stimulation.**

(A, B) The effects of the selective ARF6 inhibitor NAV-2729 on OC differentiation; scale bar, 400 μm. (C) CCK8 assay revealing the influence of NAV2729 on BMM cell viability and proliferation at different concentrations. (D-E) The overexpression of dominant negative ARF1 (T31N) and constitutively active ARF1 (Q71L) in BMMs confirmed by Western blot. (F) OC differentiation after overexpressing ARF1 (T31N) and ARF1 (Q71L); scale bar, 400 μm. (G) TRAP-positive cell count per well in each group. (H-I) The activation of ARF1 after RANKL stimulation and cytohesin-2 silencing. The active form of ARF1-GTP was detected using a commercial kit and was normalized to the total ARF1 level in the lysates. (J-K) SecinH3 suppressed RANKL-induced activation of ARF1. Cells were stimulated with RNAKL for five minutes before collection. (L, M) OC differentiation from SecinH3 treated BMMs after overexpression of ARF1 (Q71L) and the count of TRAP-positive cells per well in each group; scale bar, 400 μm. (N) The expression of ARF1 in the sham and OVX operated group by western blot and the related quantification of the blots. BMMs were obtained from the femurs of three mice per group cultured with 30 ng/mL MCSF.

Due to the overactivated features of BMMs and osteoclasts in OVX models, the BMMs were stimulated with reduced concentration of RANKL (25 ng /ml) for two days before protein collection. Statistical significance: * P < 0.05; ** P < 0.01; *** P < 0.001; **** P < 0.0001; NS, no significance. "#" indicates the control group in each comparison.

**Figure 4. SecinH3 or knockdown of cytohesin-2 suppresses podosome structure formation and reduces resorptive function of OCs.** (A) SecinH3 dose-dependently suppressed the expression of *Mmp9*, *Ctsk*, *Nfatc1*, and *TRAP* at the mRNA level. (B) SecinH3 (12 μM) suppressed the protein level of MMP9, CTSK, NFATc1, and TRAP on day 1, 3 and 5 during OC differentiation. (C-D) SecinH3 dose-dependently suppressed podosome structure formation during OC differentiation. The number of podosome structures, including podosome clusters and podosome belts were counted for each well; scale bar, 400 μm. After being fixed with 4% paraformaldehyde and permeabilized with 0.1% Triton X-100, cells were incubated with FITC- phalloidin for 30 min to show the podosome structures. The Nuclei were visualized by DAPI staining. (E-F) SecinH3 dose-dependently suppressed the resorptive function of OCs. BMMs were cultured and OCs were formed on hydroxyapatite-coated Osteo Assay strip well plates. The red arrow indicates the hydroxyapatite surface, while the black arrow indicates the resorptive region; scale bar, 400 μm. (G) Cytohesin-2 silencing inhibited the resorptive function of OCs; scale bar, 400 μm. (H, I) Knockdown of cytohesin-2 suppressed the expression of MMP9, CTSK, NFATc1, and TRAP at the protein level. BMMs were transinfected with shRNA-adenovirus targeting cytohesin-2 or the scramble-adenovirus for 12 hours and were subsequently cultured with RANKL for 3 days. Statistical significance: * P < 0.05; ** P < 0.01; *** P < 0.001; **** P < 0.0001; NS, no significance. "#" indicates the control group in each comparison.

**Figure 5. Cytohesin-2 inhibition by SecinH3 inhibits JNK pathway in the RANK signaling during osteoclastogenesis.** (A) Principal component analysis (PCA) revealed differential expression patterns between SecinH3 treated group and control group. (B) Volcano plot showing the differentially expressed genes between the control group and treatment group. A total of 447 up-regulated and 1256 down-regulated genes were identified by setting the threshold of |log2 (fold change) | to 0.5 and the P value to 0.01. (C) Heatmaps revealed that the expression of osteoclast marker genes, RANK signaling genes and inflammation-related genes was all inhibited by SecinH3. R_1 to R_3, RANKL treated groups; S_1 to S_3, SecinH3 treated groups. (D) KEGG analyses revealed that the MAPK pathway was the most significantly suppressed pathway by SecinH3. (E) Heatmaps showing the downregulated genes in the MAPK pathway by SecinH3 treatment. (F) GSEA

analysis confirmed the inhibition of the MAPK pathway by SecinH3. (G, H) Western blot assay examining the activation of the JNK, ERK and p38 branches of the MAPK pathway after SecinH3 treatment. (I, J) Western blot showing the suppression of JNK pathway after cytohesin-2 silencing. Statistical significance: * $P < 0.05$; ** $P < 0.01$; *** $P < 0.001$; **** $P < 0.0001$; NS, no significance. "#" indicates the control group in each comparison.

**Figure 6. Cytohesin-2 inhibition reduces the endoribonuclease activity of IRE1 and the UPR process.**

(A) The inhibition of *XBP1s* by SecinH3 after 8 and 16 hours of RANKL treatment. (B, C) Western blot showing the decreased protein level of XBP1s and p-IRE1 by SecinH3 treatment. (D) The inhibition of p-IRE1 by cytohesin-2 silencing. (E) SecinH3 mediated inhibition of XBP1s and p-IRE1 was reversed by the overexpression of ARF1 (Q71L). (F, G) The UPR inducer thapsigargin (TG, 0.1 nM) attenuated the inhibitory effects of SecinH3 on OC differentiation. (H, I) TG treatment attenuated the inhibitory effects of cytohesin-2 silencing on OC differentiation. (J) Pit formation assay in the RANKL, SecinH3 and SecinH3 + TG groups. (K, L) The expression of OC marker genes in the SecinH3 and SecinH3 + TG group; Cells were treated with the indicated reagents for three days in the presence of RNAKL. * $P < 0.05$; ** $P < 0.01$; *** $P < 0.001$; **** $P < 0.0001$. "#" indicates the control group in each comparison.

**Figure 7. The JNK pathway acts upstream to control the endoribonuclease activity of IRE1.**

(A, B) The suppression of OC differentiation by the JNK pathway inhibitor SP600125 (10 μM), and the IRE1 endoribonuclease activity inhibitor 4μ8C (5 μM). (C) The effect of the IRE1 endoribonuclease activity inhibitor 4μ8C on transient activation of JNK following RANKL stimulation. Cells were starved in FBS-free medium without FBS for 12 hours, followed by pre-treatment with or without 4μ8C (5 μM) for 12 hours before RANKL stimulation. The level of JNK was detected 15 min after RANKL treatment. (D) Decreased phosphorylation of IRE1 by the JNK inhibitor SP600125 after 15 min of RANKL stimulation. Cells were pre-treated with or without SP600125 (10 μM) for 12 hours before RANKL stimulation. (E) Decreased phosphorylation of IRE1 by SP600125 treatment after 8 hours of RANKL stimulation. (F) The p-IRE1 inducer TG (0.1 nM) attenuated the inhibitory effects of SP600125 on OC differentiation. Statistical significance: * $P < 0.05$; ** $P < 0.01$; *** $P < 0.001$; **** $P < 0.0001$; NS, no significance. "#" indicates the control group in each comparison.

**Figure 8. A graphical abstract for the mechanisms by which Cytohesin-2 regulates OC differentiation.** Cytohesin-2 and ARF1 mediate the activation of JNK pathway after RANKL treatment, which further regulates the endoribonuclease activity of IRE1 and promotes the IRE1/XBP1s branch of UPR, leading to osteoclast differentiation. Blocking this axis with the cytohesin-2 inhibitor SecinH3 inhibits

osteoclast differentiation. UPR, unfolded protein response.

**Supplementary figure 1.** H&E staining of the liver, heart and kidney tissues in mice of different SecinH3 dosage groups. Scale bar, 200 μm

**Supplemental figure 2.** SecinH3 has no effects on osteoblast activity and mineralization. A. The effects of SecinH3 on osteoblast mineralization revealed by alizarin red S staining. MC3T3-E1 cells were cultured in osteogenic differentiation medium with or without SecinH3 (12 μM) for 21 days before the staining assay. B. representative images of the ALP staining assay on MC3T3-E1 cells cultured with osteogenic differentiation medium for seven days. C. the expression of osteoblast related genes, such as *Alp*, *Runx2*, and *Ocn*, after SecinH3 (12 μM) treatment. MC3T3-E1 cells were cultured in osteogenic differentiation medium for seven days before the PCR test. NS, no significance. "#" indicates the control group in each comparison.

**CRediT authorship contribution statement**

FL and HFG conceived and supervised the study. YMD and KHS designed the experiments. YMD, KHS performed the experiments and analyzed the data. YMD wrote the manuscript and prepared the figure. XT drew the graphical abstract. PJW, JCG, HLK, RPP, MPZ, KXY and QG, and XW participated in the experiments and were responsible for technical, or material support.

**Graphical abstract**